Investigation on the extreme peak mooring force distribution of a point absorber wave energy converter with and without a survivability control system

Z. Shahroozi, M. Göteman, and J. Engström

***Abstract*—To determine the optimal design of the wave energy converter (WEC) that can withstand extreme wave conditions, the short- and long-term extreme responses of the system need to be determined. This paper focuses on the extreme peak force distribution of the mooring force for a 1:30 scaled point absorber WEC. The basis of this analysis is the mooring force response obtained from a WEC-Sim model calibrated by wave tank experimental data. The extreme sea states have been chosen from a 50-year environmental contour. Here, first, the long-term extreme response using the full sea state approach is obtained for three constant damping cases of the power take-off (PTO) system. Then, using a contour approach, the expected value of the extreme peak line (mooring) force distribution is computed for the sea states along an environmental contour. Further, for the most extreme sea state, the extreme peak line force distribution is also computed where a survivability control system, based on a deep neural network (DNN), changes the PTO damping to minimize the peak mooring force in each zero up-crossing episode of surface elevation. The results show that in the absence of a control system, the zero PTO damping case is a conservative choice in the analysis of the long-term response and the design load. For the most extreme sea state along the environmental contour, the survivability control system slightly reduces the expected value of the extreme peak force distribution when compared with lower constant PTO damping configurations.**

***Index Terms*—Wave energy converter, Deep neural network, Control system, Design load, Long-term extreme response.**

I. Introduction

THE design load cases (DLCs) for the highest expected loads, over the lifespan of the wave energy converters need to be identified to ascertain their survivability during extreme wave conditions. The best practices to determine the environmental design loads are outlined by international standards such as [1–3] which include recommendations such as the type of the load and environmental conditions that should be considered as well as the computation process of the extreme response distribution.

Z. S., M. G. and J. E. are affiliated with Department of Electrical Engineering, Uppsala University, Sweden (e-mail: zahra.shahroozi@angstrom.uu.se)

Digital Object Identifier:
https://doi.org/10.36688/ewtec-2023-161

To acquire the design load, the short- and long-term extreme responses have to be obtained. The former is obtained through a set of statistical methods to provide an understanding of the largest response of the device for a specific sea state and time duration. In [4], Vanem (2015) studied the uncertainties related to the extreme value analysis considering different statistical methods such as GEV, Gumbel, Weibull, Frechet, Generalized Pareto Distribution (GPD), and the average conditional exceedance rate method (ACER) for three different data set. The author concluded that there is large variability based on the extreme value analysis approach and choosing a singular method or approach that is entirely favored for this type of analysis is not a straightforward decision. On the other hand, the long-term extreme response gives information about the expected load during the lifespan of the device which can be obtained through various methods where the most common ones are the contour approach and the full sea state approach. The contour approach searches along the environmental contour line for the sea state that provides the largest response [1, 5, 6]. This method, however, is often prone to uncertainties both due to the determination of the environmental contour itself and neglecting the short-term realization of the sea states within the contour. To account for this variability, Ren et al. (2015) in [7] and Muliawan et al. (2013) in [8] recommended multiplying the expected (mean) value obtained from the short-term extreme peak force distribution of the most extreme sea state by a correction factor of 1.3, which can be determined by comparing the long-term full sea state responses with the corresponding ones from the contour approach. An alternative approach is to consider only a higher percentile of the chosen short-term extreme peak force distribution in order to address this uncertainty [1, 5]. Unlike the contour approach, the full sea state approach requires a large number of sea states from both inside and around the environmental contour line to represent the expected long-term response. Coe et al. (2018), [5], investigated the influence of the number of sea states that can be considered in the full sea state long-term approach on predicting the design response of a spheroid floater WEC. Their findings indicated that utilizing 50 sea states within the environmental contour yielded a reliable result for the given WEC. Moreover, increasing the number of sea states did not significantly

alter the predicted response level, but it did decrease the level of uncertainty in the response. Further, the importance of constructing the environmental contour is discussed by Edwards and Coe (2019) in [9] where five environmental contours, i.e. principal component analysis (PCA), Rosenblatt, Gaussian, Gumbel, and Clayton, were subjected to their studies for the two-body floater RM3 WEC. The authors noticed that for the longer wave energy periods, a larger significant wave height is predicted for the PCA method. They emphasized the importance of this observation on the design decision for mooring tension which is a low-frequency phenomenon.

The main objective and novelties of this paper are: to first compare the long-term mooring force response using the full sea state approach with 180 sea states for three constant PTO damping configurations; then, to study the effect of a survivability control system on the mooring force response and computation of the expected value of the extreme peak force distribution for the most extreme sea state identified from along the environmental contour following the contour approach. The controller is based on a deep neural network (DNN) with a similar architecture as in [10] where the control system task is to find the optimum damping that minimizes the peak force in each zero up-crossing episode of surface elevation. This study is the extension of the previous work [11] where the environmental design load was determined based on the system response of the mooring force considering only a constant PTO damping force.

The remainder of this paper is as follows: the theory and method of the wave tank experiment, WEC-Sim setup, neural network control model, and short-term and long-term extreme analysis are explained in Section II. Then, the result of the long-term extreme response and controller performance in the most extreme sea state is discussed in Section III. Finally, the conclusion of the paper is drawn in Section IV.

II. Theory and Methods

A. Wave tank experiment

To evaluate the system response of a point absorber wave energy converter during extreme wave conditions, a 1:30 wave tank experiment was conducted in the Ocean and Coastal Engineering Laboratory of Aalborg University, Denmark. The experimental setup comprised a linear sliding friction-damping power take-off (PTO), a cylindrical aluminum buoy with ellipsoidal bottom, and three pulleys to connect the buoy from the wave tank to the PTO located in the gantry via a Dyneema rope, see Fig. 1.

The PTO translator applied constant Coulomb friction damping by its vertical movement and rubbing against a Teflon block. Four damping configurations of D_0, D_1, D_2, and D_∞ were considered. The first three configurations corresponded to the sliding friction damping force of approximately 0 N, 7.4 N, and 18.9 N. In the last configuration (D_∞), the PTO was locked. Only an upper-end stop spring with a spring coefficient of 5.9 N/mm confined the PTO movement.

The inputs to the wavemaker were extreme sea states selected from an environmental contour with a 50-year return period constructed from the I-FORM hybrid method for the Dowsing site in the North Sea, see Fig. 2. The International Electrotechnical Commission (IEC) [2] recommends the use of 50-year sea states, which involve significant wave height (H_s) and peak period (T_p), as a means to simulate extreme wave conditions and assess the performance of wave energy converters during their survival mode [13]. This explains the selection of a 50-year return period as the basis of the study conducted here. The construction of the environmental contour and its rationale have been thoroughly explained in [11, 14, 15]. Note that the experiment is conducted for three different wave types of regular, irregular, and focused waves generated by wavemaker as shown in Fig. 1. Further explanation about the wave generation can be found in [16]. However, the basis of this analysis is irregular waves for sea states 5a, 6, 7, and 8.

The nonlinear phenomena such as overtopping, wave breaking, and wave breaking slamming were observed during the wave tank experiment. The overtopping phenomenon was more dominant for larger PTO damping configurations where the movement of the system was more constrained. On the other hand, the wave breaking slamming was more seen for the lower damping configuration and resulted in numerous end-stop compression. For greater details about the wave tank experiment setup and results refer to [17] and [16].

B. WEC-Sim model

To provide sufficient training set for the neural network model, data is augmented using the WEC-Sim model which is calibrated based on experimental data. The WEC-Sim model includes three one-degree-of-freedom PTOs that are connected in series to mimic the motion of the device in heave, surge, and pitch motion and to give feedback and actuation force. Note that the physical PTO is a linear friction system that moves vertically, in contrast to the WEC-Sim PTO which are simulation blocks that restrict the motion of the buoy in three degrees of freedom.

The weakly nonlinear effect of the buoy's dynamic is captured by computing the nonlinear buoyancy and Froude-Krylov forces. The drag coefficient in heave is computed based on curve fitting of the decay test from experimental to numerical WEC-Sim through the least square method. To obtain the surge drag coefficient, the amplitude response operator (RAO) in WEC-Sim is adjusted to match the experimental RAO. The pitch drag coefficient is determined by calibrating the WEC-Sim buoy motion in pitch, using the experimental data collected from the Qualisys camera as a reference for the regular waves. This is accomplished through the application of the least square method [11].

By examining the power take-off (PTO) from the buoy side and analyzing the equation of motion in vector form, the WEC-Sim line (mooring) force is characterized as [11]:

$$m_{\text{PTO}}\ddot{\mathbf{z}}_{\text{PTO}} = \mathbf{F}_{\text{line}} + \mathbf{F}_{\text{endstop}} + \mathbf{F}_{f_{\text{PTO}}} + \mathbf{F}_{fp} + m_{\text{PTO}}\mathbf{g} \quad (1)$$

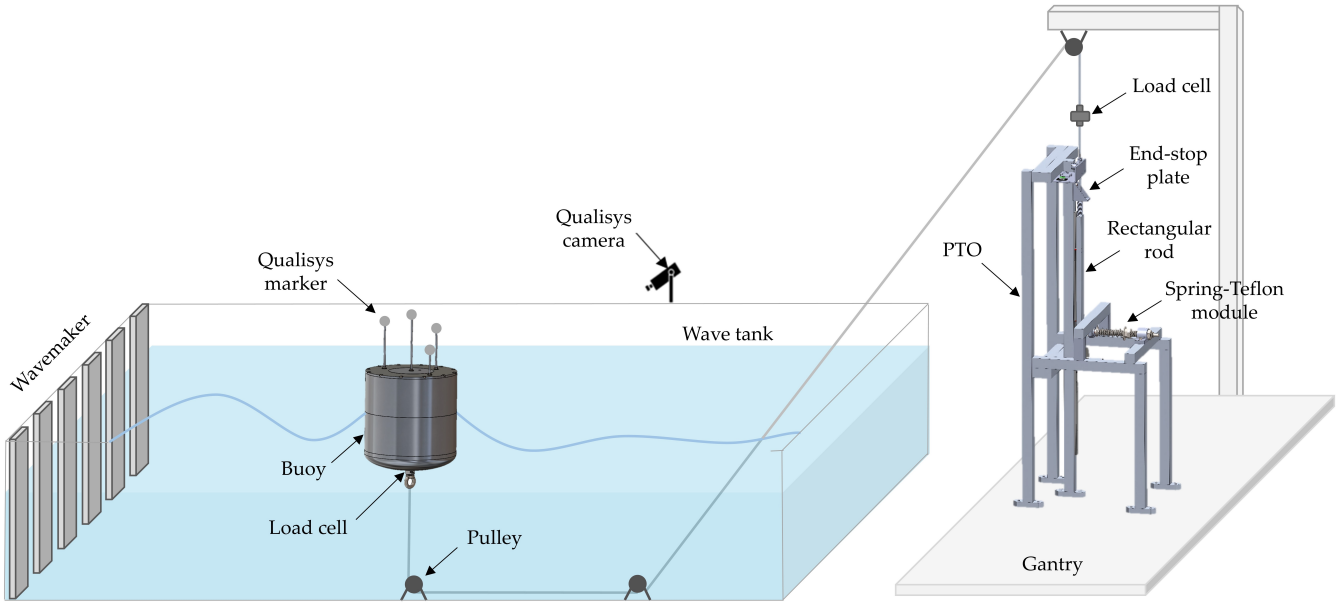

Fig. 1: The schematic of the wave tank experiment, retrieved from [12].

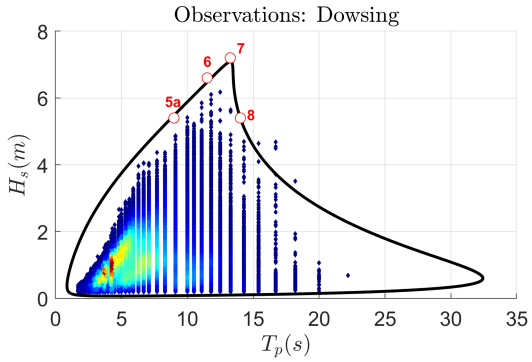

Fig. 2: The environmental contour constructed with the I-FORM hybrid method with a 50-year return period for the Dowsing site in the North Sea. In this paper, in part of the analysis, i.e. the contour approach, sea state 5a, 6, 7, and 8 are considered from which sea states 5a, 6, and 8 were experimented in the wave tank, adapted from [15].

where the total mass of the translator, including its attachment, is represented by m_{PTO}. The forces of the end-stop spring, PTO friction, and pulley friction are denoted by $\mathbf{F}_{\text{endstop}}$, $\mathbf{F}_{f_{\text{PTO}}}$, and $\mathbf{F}_{fp}$ respectively. Additionally, the PTO acceleration and gravitational acceleration are represented by $\ddot{\mathbf{z}}_{\text{PTO}}$ and $\mathbf{g}$ respectively.

From the instantaneous position of the buoy and F_{line}, the force actuation of the PTO WEC-Sim blocks is determined. See [11] and the equations 8-10 therein for the derivation of the surge and heave forces and pitch moment.

The PTO force for WEC-Sim (1) is represented as a combination of static friction, Stribeck, and Coulomb components as a function of relative velocity [18]:

$$F_{f_{\text{PTO}}} = \sqrt{2e}(F_{\text{brk}} - F_{C_{\text{PTO}}})\exp\left(-\left(\frac{\dot{z}_{\text{PTO}}}{v_{\text{St}}}\right)^2\right)\frac{\dot{z}_{\text{PTO}}}{v_{\text{St}}} + F_{C_{\text{PTO}}}\tanh\left(\frac{\dot{z}_{\text{PTO}}}{v_{\text{Coul}}}\right) \quad (2)$$

where the breakaway friction and Coulomb forces are denoted by F_{brk} and $F_{C_{\text{PTO}}}$, respectively. Additionally, the Stribeck velocity is defined as $v_{\text{St}} = v_{\text{brk}}\sqrt{2}$, where v_{brk} is the velocity at which the breakaway friction occurs. The Coulomb velocity threshold is defined as $v_{\text{Coul}} = v_{\text{brk}}/10$. The relative velocity is denoted by $\dot{z}_{\text{PTO}}$, and Euler's number is represented by e.

The pulley friction force in the WEC-Sim model is also modeled as a function of velocity based on only the Coulomb component:

$$F_{fp} = F_{C_p}\tanh\left(\frac{\dot{z}_{\text{PTO}}}{v_{\text{Coul}}}\right) \quad (3)$$

where the Coulomb force is represented as $F_{C_p} = \mu_p F_{\text{line}}$, with μ_p being the friction coefficient of the pulley. The value of this coefficient was determined through a series of simple experiments in which the translator was manually moved downwards at a nearly zero velocity, while both load cells at the buoy and PTO side measured the force. By subtracting the measured forces from both sides, the pulley friction force was calculated. Then, the pulley friction coefficient was obtained based on the proportionality of the pulley friction force to the line (mooring) force measured by the load cell attached to the buoy [11].

The end-stop force in the WEC-Sim model is represented as an elastic end-stop module:

$$F_{\text{endstop}} = \begin{cases} k_{\text{es}}(l_0 - l_{\text{c}}) + k_{\text{st}}\left(z - \frac{l_{\text{s}}}{2}\right) + c_{\text{st}}\dot{z}, & (i) \\ k_{\text{es}}(l_0 - l_{\text{c}}) + k_{\text{st}}\left(z - \frac{l_{\text{s}}}{2}\right), & (ii) \\ k_{\text{es}}\left(z - \left(\frac{l_{\text{s}}}{2} - (l_0 - l_{\text{c}})\right)\right), & (iii) \end{cases} \quad (4)$$

where (i) is for $z > l_{\text{s}}/2$, and $\dot{z} > 0$, (ii) is for $z > l_{\text{s}}/2$, and $\dot{z} \leq 0$, and (iii) is for $l_{\text{s}}/2 - (l_0 - l_{\text{c}}) < z \leq l_{\text{s}}/2$. The end-stop spring coefficient is k_{es}, and the equivalent spring coefficient of the structure is represented by k_{st}. The initial and compressed lengths of the end-stop spring are denoted by l_0 and l_c, respectively.

Additionally, the energy dissipated after the spring is fully compressed is modeled as a viscous damper with the coefficient c_{st}, for $\dot{z} > 0$. For more information on the setup of WEC-Sim model, refer to [11].

The performance of WEC-Sim model is evaluated by comparing the empirical cumulative distribution function (ECDF) of the peak line forces obtained from WEC-Sim simulations and experiments. The reader can refer to [10, 11] to see the performance of the WEC-Sim model versus experimental data. The simulations are conducted using 20 different seeds, each with a duration of 0.18 hours for each damping configuration for the 1:30 scaled model. This amounts to approximately 11 hours of system response that is fed into the neural network model for training. It should be noted that the locked PTO case was not studied due to the inability of the WEC-Sim model to reproduce the system response for such a complex case, where nonlinear phenomena such as overtopping and frequent slack in the line rope were observed during the experimental campaign [10]. The analysis of WEC-Sim is conducted on a high-performance computing (HPC) cluster that is provided by Uppsala Multidisciplinary Center for Advanced Computational Science (UPPMAX).

C. Neural network model

A deep neural network (DNN) structure is created to serve as a core of the control system with the purpose of forecasting the maximum line (mooring) force in each sea state, to identify the ideal damping that reduces the peak line force. The peak line forces are selected for each zero up-crossing episode of surface elevation. The DNN model is built using Keras in Python, which runs on the TensorFlow machine learning framework. The training of the model is performed on a regular laptop, which takes only a few minutes [10].

The neural network model consists of eight input features extracted from WEC-Sim model responses: the Coulomb force (i.e. sliding friction force), maximum wave amplitude, wave period, the initial value of the translator position, velocity, and acceleration, and the initial and maximum value of the derivative of surface elevation for each zero up-crossing episode of the surface elevation. The outputs of the network are the peak line force value and its probability of extremity, i.e. being above a certain threshold, in each episode. The DNN model architecture is shown in Fig. 3. The flowchart of the control system is shown in Fig. 4. The optimization loop task is to provide a range of sliding friction-damping forces to the neural network model to identify the minimum peak line force and its corresponding damping force. The training and test data set to the DNN model are the WEC-sim peak mooring force for sea state 7 considering 20 seeds for three damping configurations of D_0, D_1, and D_2. The 80% of the available data is considered to train the DNN model, and the rest is used to assess the generalization and performance of the model.

The DNN model performs both regression and classification tasks, with the latter aiding the regression

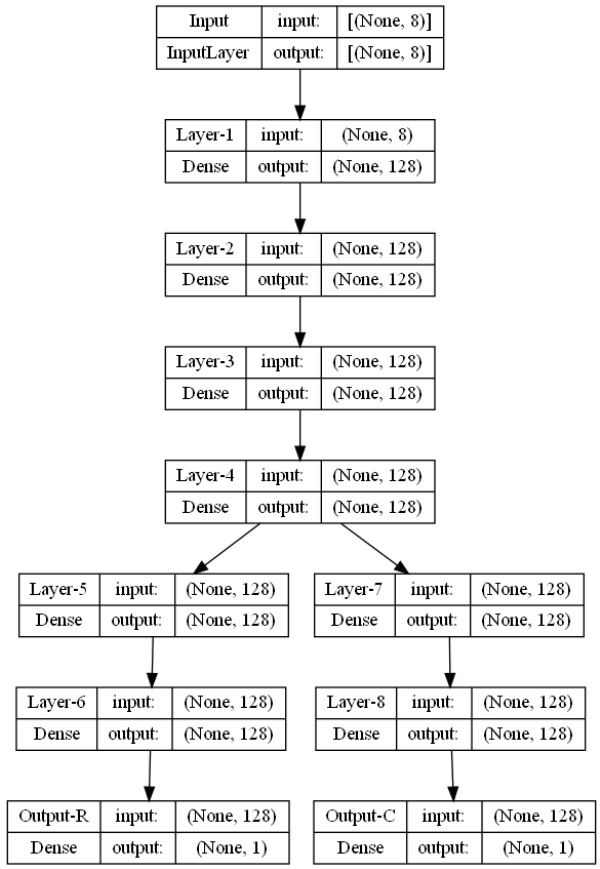

Fig. 3: The architecture of the deep neural network where the output of regression and classification tasks are shown as "Output-R" and "Output-C", respectively.

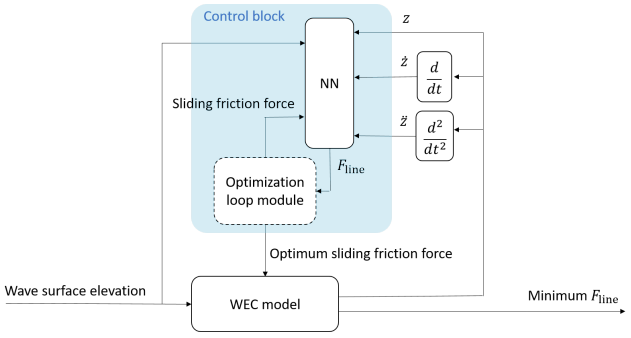

Fig. 4: The DNN control system flowchart. The sliding force refers to the PTO constant coulomb friction force, adopted from [10].

problem through an attention mechanism that focuses on extreme forces exceeding a certain threshold. The attention mechanism is introduced as: $y_p = \hat{y} + \zeta\tilde{y}$ in which the predicted peak line force is y_p, the output of the network from the regression task is $\hat{y}$, and the predicted probability of the extreme peak line force above a threshold of 150 N is denoted as $\tilde{y}$. Note that this threshold is selected based on visual observation of the maximum forces in the most extreme sea states. The attention factor (ζ) is a trainable parameter of the network that emphasizes extreme events. The training model is described in the following algorithm [10]:

The model is first trained to minimize the classifi-

Initialize: parameters θ, and ζ
for *each epoch* **do**
  for *each training batch* **do**
    Minimize BCE loss function $J_1(\theta)$
  end
  for *each training batch* **do**
    Calculate peak line force, $y_p = \hat{y} + \zeta\tilde{y}$ from network outputs $(\hat{y}, \tilde{y})$
    Minimize MARE loss function $J_2(\theta, \zeta)$
  end
end

Algorithm 1: Training algorithm of the proposed DNN.

TABLE I: The hyperparameters of the DNN model.

Number of nodes	128
Activation hidden layer	PReLU
Activation output layer classification	Sigmoid
Activation output layer regression	ReLU
Regularization	L2
Optimization method	Adam
Batch size	256

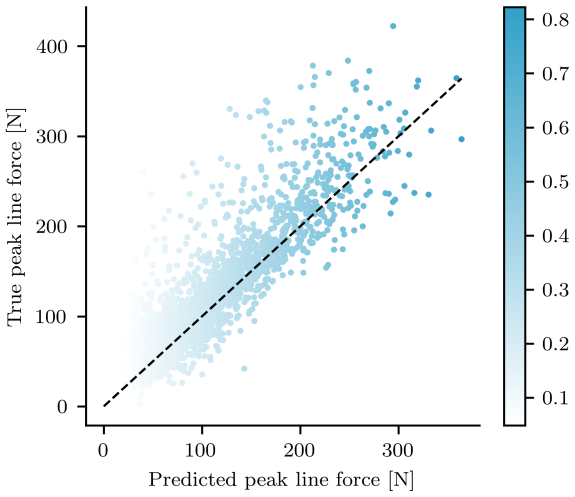

Fig. 5: The performance of the DNN model for the regression task is demonstrated by comparing the predicted and true peak line forces. The color bar represents the probability of extreme forces, with higher probabilities indicating larger peak line forces.

cation loss function, i.e. considered as Binary Cross Entropy (BCE), and then minimizes the regression loss that is taken as the mean absolute relative error (MARE). The accuracy of the model is computed as 1-MARE as:

$$\text{accuracy} = 1 - \frac{1}{n}\sum\left|\frac{y_t - y_p}{y_t}\right| \tag{5}$$

where n is the number of data points, and the true and predicted peak line forces are y_t and y_p, respectively. The hyperparameters of the DNN model are given in Table I. The description of these parameters is provided in [10, 19].

The performance of the DNN model on the test data set is shown in Fig. 5 which depicts the correlation between the true (WEC-Sim) and predicted peak line force obtained from the regression task with an accuracy (1-MARE) of 84%. Although the attention mechanism improves the prediction of the peak line forces, the DNN performance suggests that more complex attention mechanisms can be beneficial to capture the high peak forces in the most extreme sea states such as sea state 7 here.

Then, the trained network is integrated into the control block of the WEC-Sim model where the Coulomb (sliding) friction-damping force is ranged from 0.0 to 20 N in 1.0 N increments. To maintain the neural network's accuracy, specifically larger damping values than the experimental ones that the WEC-Sim model is calibrated on, are not considered. For a greater explanation of this control system refer to [10].

D. Short-term extreme response

The short-term extreme response provides information on the maximum response of a device, such as the bending moment or mooring line force, that can be expected during a specific sea state and time period, usually equivalent to a storm duration of 1 to 3 hours during which the spectral density function of the sea state is assumed to remain constant [5, 20].

To assess short-term extreme value distribution, the peak-over-threshold method is employed. This method investigates the upper tail of peak line (mooring) force distribution above a certain threshold (u) that is selected for each sea state individually. The outline of this method is provided as follows [11]:

i. Select the peak line forces (x_p) between two consecutive zero up-crossing of the surface elevation.
ii. Choose a certain threshold for each sea state. In the contour approach (i.e. later explained in subsection II-E) where a few sea states are considered, the appropriate threshold for each sea state is identified through the mean residual life plot, and the scale and shape parameters stability plots. However, in the full sea state approach where a large number of sea states should be taken into account, the threshold for each sea state is computed as: $\mu_{x_p} + 1.4\sigma_{x_p}$ where the mean and standard deviation of peak forces are μ_{x_p} and σ_{x_p}, respectively, under the condition that the number of exceedances is more than 20 and the shape parameter is negative. If the condition is not met, the threshold value is progressively lowered until the criteria are satisfied. A great discussion about the methods mentioned in this step is presented in [11].
iii. Fit the generalized Pareto distribution given in (6) to the exceedances of the peak line force ($z_p = x_p - u$ for $x_p > u$):

$$P_{\text{GPD}}(z_p) = \begin{cases} 1 - \left(1 + \frac{kz_p}{\alpha}\right)^{-\frac{1}{k}}, & k \neq 0, 1 + \frac{kz_p}{\alpha} > 0 \\ 1 - \exp\left(-\frac{z_p}{\alpha}\right), & k = 0, z_p > 0 \end{cases} \tag{6}$$

where α and k are the scale and shape parameters, respectively. The distribution can be approximated

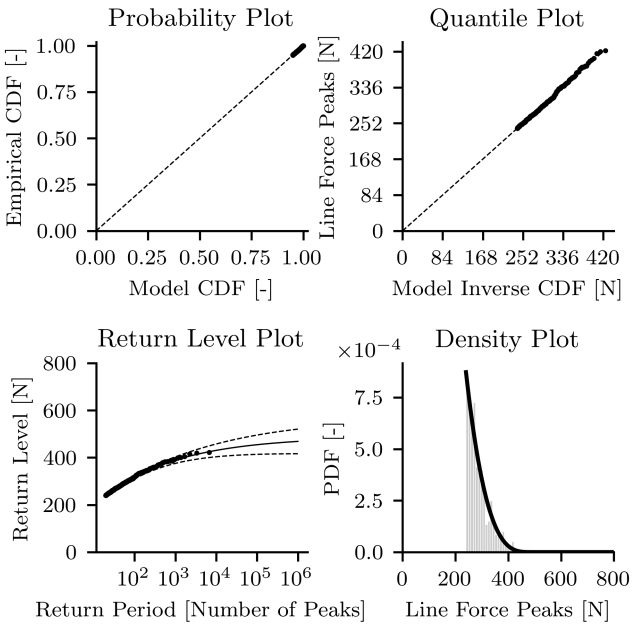

Fig. 6: Diagnostic plots for the peak forces with the control system using GPD fit for sea state 7.

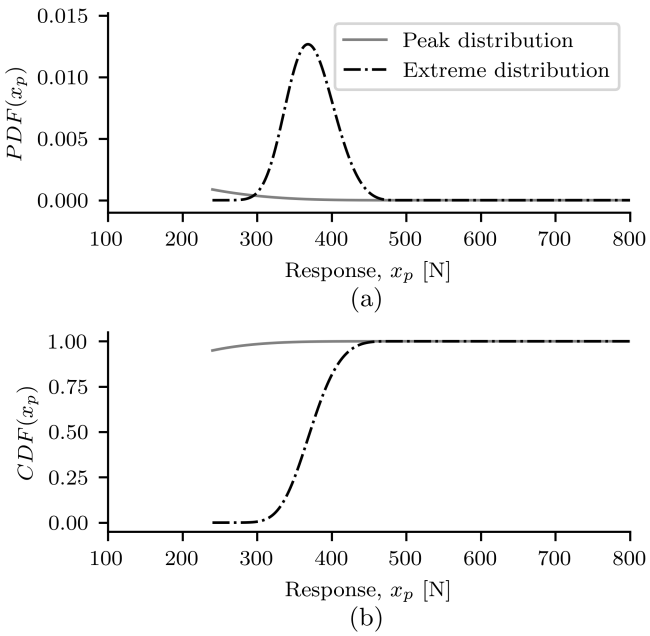

Fig. 7: The probability density function (PDF) (in sub-figure (a)) and the cumulative distribution function (CDF) (in sub-figure (b)) of the peak and extreme distributions of the line forces with the control system for sea state 7 using GPD fit.

as the exponential distribution in the special case of $k = 0$. The distribution of exceedances has an upper bound of $u - \alpha/k$ for $k < 0$, whereas, there is no upper limit for $k > 0$, [21].

iv. Compute the cumulative distribution function (CDF) of the peak line force on the basis of the CDF of exceedances [5, 6, 11, 20]:

$$P_{P,\mathrm{GPD}}(z_P + u) = 1 - \left(\frac{N_{\mathrm{pot}}}{N}\left(1 - P_{\mathrm{GPD}}(z_P)\right)\right) \quad (7)$$

where N and N_{pot} are the total number of peak line force and the number of peaks above the certain threshold that is selected for each sea state respectively.

v. Calculate the short-term extreme CDF based on the CDF of peaks obtained in (7) as [6, 11, 20, 22]:

$$P_{st}(x) = P_{P,\mathrm{GPD}}(x)^{N_{st}} \quad (8)$$

where in each 0.18-hour short-term extreme simulation period (Δt_{st}), i.e. corresponding to 1-hour for the full-scale system, the average number of peak line force is $N_{st} = N(\Delta t_{st}/\Delta t)$ in which the total simulation length, Δt, is 20×0.18.

For discussion about the selection of peak-over-threshold method in this case over other statistical methods for the analysis of short-term extreme response refer to [11].

Fig. 6 shows that the GPD fit excellently captures the tail distribution of the peak forces data above the threshold of 240 N for sea state 7 considering the system response with the survivability controller. This can be seen by looking at the quantile and probability plots where the peak line force above the threshold follows the diagonal line very well. Moreover, the extreme and peak distributions of this system's response are illustrated in Fig. 7.

E. Long-term extreme response

The analysis of long-term extreme response provides insight into the expected loads and system response of an offshore system during its deployment life for a specific environmental condition. The long-term extreme response analysis can be conducted using two well-known methods: full sea state approach and contour approach [11].

1) Full sea state approach: This approach provides an accurate and thorough response distribution; however, it comes at the expense of extensive computational time. This method requires a large number of sea states (H_s and T_p) selected from the environmental contour to represent the expected long-term response distribution. The distribution can then be computed as [1, 8, 11, 22]:

$$\bar{P}_{lt}(x) = \int_{h_s}\int_{t_p} \bar{P}_{st|H_s,T_p}(x|h_s,t_p)p_{H_s,Tp}(h_s,t_p)dt_p dh_s \quad (9)$$

where the occurrence probability distribution of a specific sea state is stated as $p_{H_s,Tp}$. Moreover, the so-called complementary cumulative distribution function (CCDF) or short-term survival function of the response (X) is expressed as $\bar{P}_{st|H_s,T_p}$, and it is described as [11]:

$$\bar{P}_{st}(x) = p(X > x) = 1 - P_{st}(x) \quad (10)$$

where the short-term cumulative distribution function is nominated as $P_{st}(x)$ for sea states with 0.18 hours simulation.

Here, 180 sea state samples are considered to study the full sea state approach. The sensitivity of this analysis to the number of sea states is discussed in [11]. The selection of the sea states is explained in the following steps [5, 11]:

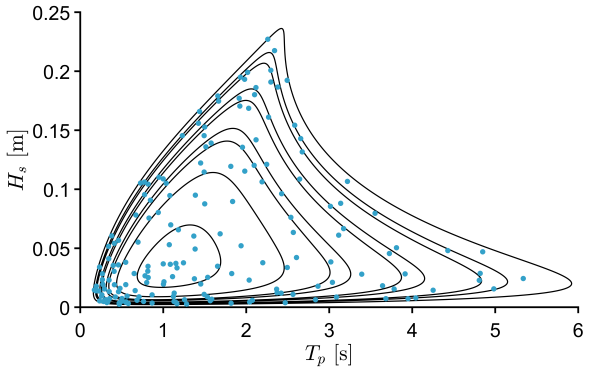

Fig. 8: The selected 180 sea states are illustrated in H_s and T_p space. The contour lines are the translation of 0.001, 0.01, 0.05, 0.1, 0.5, 1, 5, 10, and 50 years return period from full-scale to the small-scale system.

i. Construct the normal standard space (u-space) for different return periods. Here, 0.001, 0.01, 0.05, 0.1, 0.5, 1, 5, 10, and 50 years return periods are considered for the full-scale system and are then scaled down for constructing the small-scale contours.
ii. Select an equal number of sea states, i.e. 20 samples here, between each return period. Given 9 return periods that are considered in step (i.), the total number of sea states would be $20 \times 9 = 180$.
iii. Transform back the sea states from u-space to H_s and T_p space using the Rosenblatt transformation, see Fig. 8.

The equations for the u-space and Rosenblatt transformations are described in detail in [11], equations (1) to (7) therein.

2) Contour approach: This approach focuses on identifying specific sea states along the environmental contour that contribute to the maximum characteristic responses [1, 22]. Here, 20 seeds of simulations are considered for sea states 5a, 6, 7, and 8 along the environmental contour. The procedure involves several steps:

i. Calculate the short-term extreme response distribution for the sea states located along the environmental contour.
ii. Determine the expected value (mean) of these distributions to pinpoint the sea state associated with the highest response.
iii. Select the distribution with the maximum expected value and utilize a percentile of that distribution as the long-term response.

Compared to the full sea state method, this approach often requires less simulation time since it only needs to analyze a small number of carefully chosen sea states.

Note that the short-term and long-term analyses in this study are inspired by the WDRT code [22] and have been modified to suit the specific analysis conducted in this study.

III. Result and Discussion

Fig. 9 shows the survival function for each individual sea state in addition to the full sea state survival function shown by the black line which is the weighted average of the CCDF for all sea states. As mentioned in Section II, GPD is used to model the short-term distribution of each sea state above a certain threshold, and hence, the full sea state survival function (CCDF) is depicted above the maximum threshold of all sea states. Looking at the return period of 9.1 years, the return level is almost similar for damping configurations of D_0 and D_1, however, it is significantly lower for the D_2 case. This result suggests that the lower damping configurations are more conservative choices if the environmental design loads need to be calculated with a constant damping configuration. To put this in perspective, for instance, the environmental design load in the D_0 configuration for a 9.1-year return period can be computed by multiplying the return level with the load safety factor of 1.35 suggested by [1], i.e. $498.15\ \text{N} \times 1.35 = 672.50\ \text{N}$. In the full-scale system, this corresponds to 670.50 N $\times 30^3$ = 18.16 MN design load (for the D_0 case), i.e. compared with 16.23 MN in the D_2 case, for a return period of 9.1 $\times 30^{0.5} \approx$ 50 years. Note that the load safety factor of 1.35 is advocated by international standards to be multiplied with the long-term extreme response in the analysis of the ultimate limit state (ULS) for the extreme load conditions [23, 24].

As mentioned in Section II, the contour approach limits the computation of system response to a few sea states along the environmental contour and through identifying the most extreme sea state by computation of the expected value of the short-term extreme distribution. Following this, the expected value of the extreme peak force distribution for sea states 5a to 8 along the environmental contour has been investigated given the GPD fit, see Fig. 10. Lower damping cases are demonstrating the largest expected value of the extreme distribution, which is aligned with observations in the full sea state approach that the lower damping cases result in a larger long-term response. Further, in all constant damping cases, sea state 7 displays the largest expected value with the exception of the D_0 case where sea state 6 shows a similar expected value as sea state 7. Hence, sea state 7 is identified as the most extreme sea state.

Given this most extreme sea state, the influence of a control system on lowering the expected forces is evaluated in sea state 7 considering 20 seeds. Table II indicates that the control system described in subsection II-C has slightly reduced the expected value when compared with constant damping cases of D_0, and D_1. In the constant damping case of D_2 however, the expected value is lower than the control case. This does not necessarily imply that larger damping values should be adopted for survivability purposes. In larger damping configurations, the movement of the buoy is more restrained, and thereby, it is more susceptible to the overtopping phenomenon which leads to a reduction of mooring force. This has been shown in [16] where looking at the entire history of mooring force for tested sea states, the peak line force was reduced when the damping was increased up to a certain level, above which the peak force increases again drastically

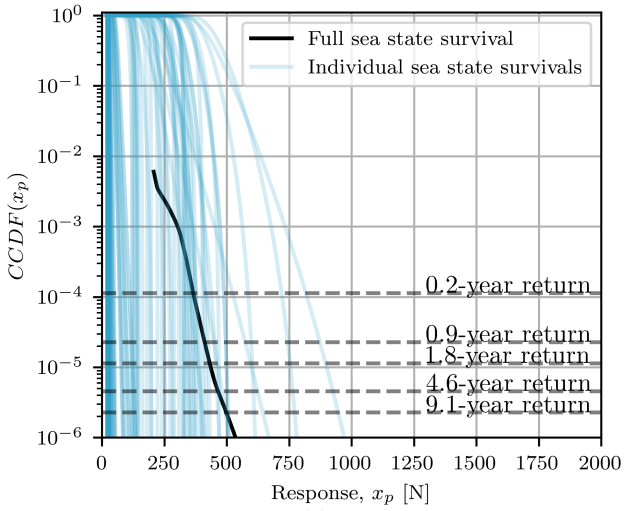

(a)

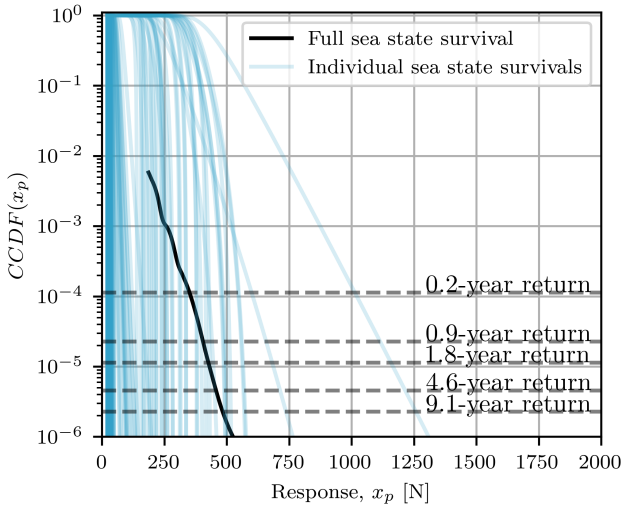

(b)

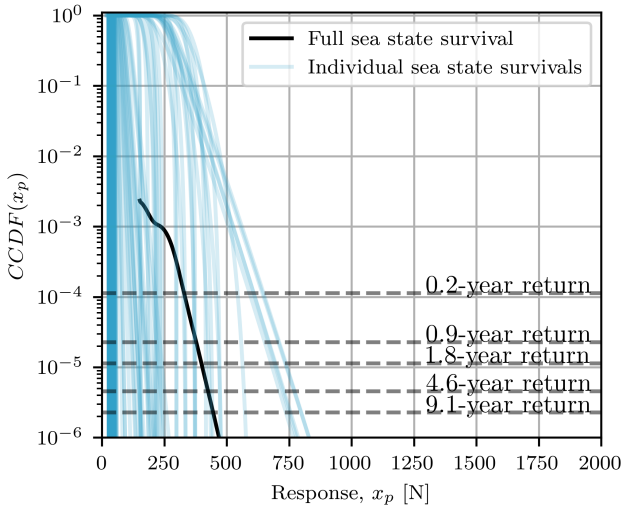

(c)

Fig. 9: subfigures (a), (b), and (c) show the survival function for constant damping cases f D_0, D_1, and D_2, respectively. The blue lines show the CCDF for 180 sea states while the black line shows the full sea state survival function. The dashed lines show different survival levels of 0.2, 0.9, 1.8, 4.6, and 9.1 years corresponding to 1, 5, 10, 25, and 50 years, respectively, in the full-scale system.

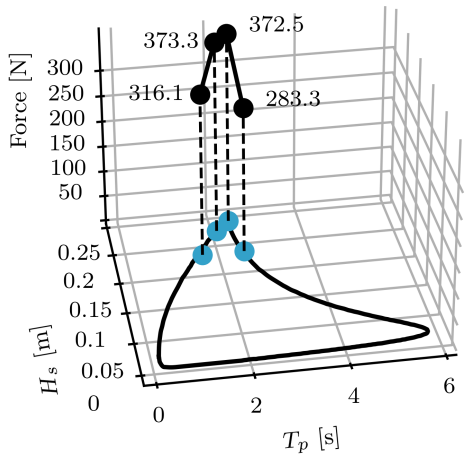

(a)

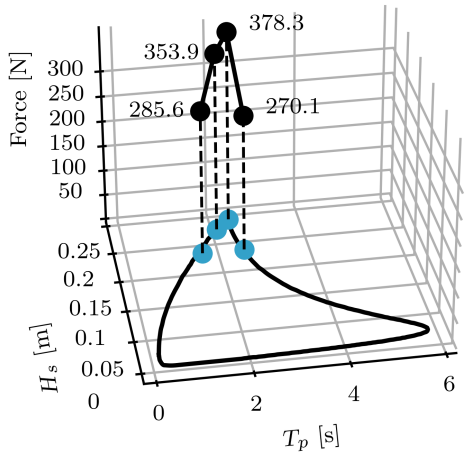

(b)

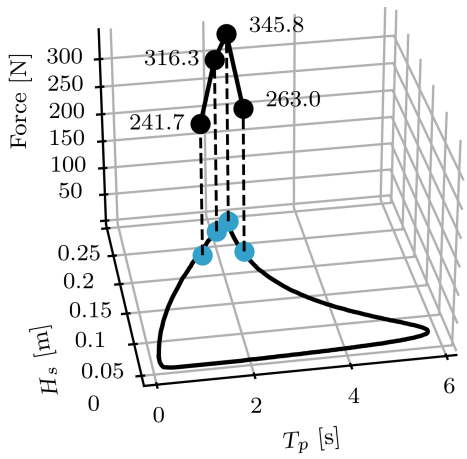

(c)

Fig. 10: The expected value of the extreme peak force distribution for sea state 5a, 6, 7, and 8 is shown for constant damping cases of D_0, D_1, and D_2 in subfigures (a), (b), and (c), respectively.

TABLE II: The expected values of the extreme peak force distribution of sea state 7 for constant PTO damping cases of D_0, D_1, and D_2, as well as the case with the control system.

Damping case	D_0	D_1	D_2	Control system
Expected value of the extreme distribution	372.5 N	378.5 N	345.8 N	367.4 N

due to high relative velocity between water and the buoy. Note that during the experiment, the overtopping was not measured and the survivability control only considers the mooring force. The possible reason that the control system did not significantly reduce the mooring force in comparison to lower damping configurations of D_0 and D_1 (i.e. identified as more critical damping cases following the results from the full sea state approach) are: 1) due to the accuracy of the DNN model, the optimal damping has not been selected correctly for some instances, and therefore, the resultant line force is higher; nevertheless, the performance of this controller with similar architecture has been investigated thoroughly in [10] and it is shown that there have been only a few times in 658 s duration of sea state 8 that the controller failed to reduce the peak line force; 2) as also explained in [10], the existence of any control system alters the system response, and the new system state at some zero up-crossings of surface elevation might dictate higher forces regardless of the choice of damping or control system. Note that the model studied here does not account for any impacts caused by biofouling, and therefore, the inclusion of this factor can be of interest for future studies.

IV. Conclusion

This paper investigates the extreme response distribution of a point absorber wave energy converter by looking at the long-term response using the full sea state approach and the expected value of the short-term extreme response following the contour approach for three constant PTO damping configurations (i.e. corresponding to sliding damping friction force of 0 N, 7.4 N, and 18.9 N). Moreover, for the most extreme sea state, the expected value of the extreme peak force distribution is also computed with a control system that adjusts the PTO damping.

The mooring force response is constructed from a WEC-Sim model that has been calibrated by experimental data. The model is used to simulate the system response for the sea states considering a 50-year environmental contour following the advocacy of the International Electrotechnical Commission (IEC). The full-state approach considers the generalized Pareto distribution (GPD) to model the short-term extreme peak force distribution and survival function of the system response for 180 sea states within the environmental contour for constant PTO damping cases. The most extreme sea state (sea state 7) is then identified along the environmental contour with the highest expected value following the contour approach. For this most extreme sea state, a control strategy is implemented based on adjusting the PTO damping through a deep neural network to minimize the mooring forces. The control system pursues two tasks of classification and regression to predict the peak line (mooring) force in each zero up-crossing episode of surface elevation.

This study is an extension of our previous work, [11], where the focus has been on the calculation of the environmental design load and the long-term response only considering one damping configuration. Here, extending the analysis to a broader PTO damping range, the long-term extreme response is compared in different constant PTO damping scenarios to find the most conservative case in the computation of the long- and short-term extreme responses and eventually the design load. The results indicate that in the case of a no-control system, the full sea state survival function and expected value of extreme peak force distribution are reduced by increasing the constant damping which implies the sensitivity of the analysis to damping of the system. This observation is especially important and infers that the most conservative choice to determine the design load is the lower damping cases close to zero.

Further, the control response has been investigated for the most extreme sea state (i.e. sea state 7) and shows the reduction of the expected value of extreme peak force distribution when comparing with the constant D_0 and D_1 cases. However, the control system was not able to provide a lower expected value of the extreme peak force distribution than the D_2 case.

Acknowledgement

This research is supported by the Swedish Energy Agency (project number 47264-1), the Swedish Research Council (grant number 2020-03634), and StandUp for Energy as well as Liljewalchs scholarships.

References

[1] G. DNV, "Environmental conditions and environmental loads (dnv-rp-c205)," *Det Norske Veritas AS, Oslo*, 2014.

[2] IEC, "Marine energy-wave, tidal and other water current converters - part 2: Design requirements for marine energy systems," *IEC TS 62600-2:2016-08*, 2016.

[3] I. E. Commission *et al.*, "Wind energy generation systems-part 3-1: Design requirements for fixed offshore wind turbines," 2019.

[4] E. Vanem, "Uncertainties in extreme value modelling of wave data in a climate change perspective," *Journal of Ocean Engineering and Marine Energy*, vol. 1, no. 4, pp. 339–359, 2015.

[5] R. G. Coe, C. Michelen, A. Eckert-Gallup, and C. Sallaberry, "Full long-term design response analysis of a wave energy converter," *Renewable Energy*, vol. 116, pp. 356–366, 2018.

[6] R. G. Coe, C. Michelen, A. Eckert-Gallup, N. Martin, Y.-H. Yu, J. van Rij, E. W. Quon, L. Manuel, P. Nguyen, T. Esterly, B. Seng, Z. Stuart, and J. Canning. (2018) WEC Design

Response Toolbox (WDRT). [Online]. Available: http://wec-sim.github.io/WDRT

[7] N. Ren, Z. Gao, T. Moan, and L. Wan, "Long-term performance estimation of the spar–torus-combination (stc) system with different survival modes," *Ocean engineering*, vol. 108, pp. 716–728, 2015.

[8] M. J. Muliawan, Z. Gao, and T. Moan, "Application of the contour line method for estimating extreme responses in the mooring lines of a two-body floating wave energy converter," *Journal of Offshore Mechanics and Arctic Engineering*, vol. 135, no. 3, 2013.

[9] S. J. Edwards and R. G. Coe, "The effect of environmental contour selection on expected wave energy converter response," *Journal of Offshore Mechanics and Arctic Engineering*, vol. 141, no. 1, 2019.

[10] Z. Shahroozi, M. Göteman, and J. Engström, "Control of a point absorber wave energy converter in extreme wave conditions using a deep learning model in wec-sim," *IEEE/MTS Oceans 2023 Limerick, 5th-8th June 2023 (accepted to be published)*.

[11] Z. Shahroozi, M. Göteman, E. Nilsson, and J. Engström, "Environmental design load for the line force of a point-absorber wave energy converter," *Applied Ocean Research*, vol. 128, p. 103305, 2022.

[12] Z. Shahroozi, M. Göteman, and J. Engström, "Fatigue analysis of a point-absorber wave energy converter based on augmented data from a wec-sim model calibrated with experimental data," *Trends in Renewable Energies Offshore*, pp. 925–933, 2022.

[13] V. S. Neary, R. J. Y. An, R. G. Coe, S. Ahn, A. Haselsteiner, L. Stroer, and K. Windmeier, "Design load case (dlc) generator: Web-based tool to determine iec 62600-2 standard design load requirements." Sandia National Lab.(SNL-NM), Albuquerque, NM (United States), Tech. Rep., 2021.

[14] L. Wrang, E. Katsidoniotaki, E. Nilsson, A. Rutgersson, J. Rydén, and M. Göteman, "Comparative analysis of environmental contour approaches to estimating extreme waves for offshore installations for the baltic sea and the north sea," *Journal of Marine Science and Engineering*, vol. 9, no. 1, p. 96, 2021.

[15] E. Katsidoniotaki, E. Nilsson, A. Rutgersson, J. Engström, and M. Göteman, "Response of point-absorbing wave energy conversion system in 50-years return period extreme focused waves," *Journal of Marine Science and Engineering*, vol. 9, no. 3, p. 345, 2021.

[16] Z. Shahroozi, M. Göteman, and J. Engström, "Experimental investigation of a point-absorber wave energy converter response in different wave-type representations of extreme sea states," *Ocean Engineering*, vol. 248, p. 110693, 2022.

[17] ——, "Experimental results of force measurements from a scaled point absorbing wave energy converter subjected to extreme waves," in *Proceedings of the Fourteenth European Wave and Tidal Energy Conference (EWTEC)*, 2021.

[18] B. Armstrong-Helouvry, *Control of machines with friction*. Springer Science & Business Media, 2012, vol. 128.

[19] Z. Shahroozi, M. Göteman, and J. Engström, "A neural network approach to minimize line forces in the survivability of the point-absorber wave energy converters," in *Proceedings of the 42nd Ocean, Offshore and Arctic Engineering Conference (OMAE 2023), accepted, under publication*, 2023.

[20] C. Michelen and R. Coe, "Comparison of methods for estimating short-term extreme response of wave energy converters," in *OCEANS 2015 - MTS/IEEE Washington*, 2015, pp. 1–6.

[21] S. Coles, J. Bawa, L. Trenner, and P. Dorazio, *An introduction to statistical modeling of extreme values*. Springer, 2001, vol. 208.

[22] R. G. Coe, C. Michelen, Y.-H. Yu, J. V. Rij, and A. C. Eckert-Gallup, "Wdrt: A toolbox for design-response analysis of wave energy converters." Sandia National Lab.(SNL-NM), Albuquerque, NM (United States), Tech. Rep., 2016.

[23] DNVGL, "Dnvgl-st-0164: Tidal turbines," 2015.

[24] H. Buckland, J. Hemmant, J. Meason, and H. Gaviglio, "An adaptation of design load cases for a wave energy converter," in *Proceedings of the Fourteenth European Wave and Tidal Energy Conference*, D. Greaves, Ed. University of Plymouth, UK: EWTEC, Sep 5–9 2021, pp. 1941-1–1941-5, ISSN: 2309-1983.